C–H Bond Activation of Methane via σ–d Interaction on the IrO2(110) Surface: Density Functional Theory Study

ARTICLE *in* THE JOURNAL OF PHYSICAL CHEMISTRY C · JANUARY 2012

Impact Factor: 4.77

1 AUTHOR:

Jyh-Chiang Jiang

National Taiwan University of Science and Tec…

174 PUBLICATIONS **2,612** CITATIONS

THE JOURNAL OF PHYSICAL CHEMISTRY C

Article

pubs.acs.org/JPCC

C−H Bond Activation of Methane via σ−d Interaction on the IrO_2(110) Surface: Density Functional Theory Study

Chia-Ching Wang, Shih Syong Siao, and Jyh-Chiang Jiang*

Department of Chemical Engineering, National Taiwan University of Science and Technology, 43, Keelung Road, Section 4, Taipei, 106, Taiwan

Supporting Information

ABSTRACT: The adsorption and dissociation of methane on the IrO_2(110) surface were investigated by density functional theory calculations. The adsorption energy of methane obtained in this study is −0.41 eV on the stoichiometric surface and −0.63 eV on the oxygen-rich surface, which are significantly higher than those calculated recently on other different catalytic systems. Analyses from density of states and electron density difference show a special interaction between the C−H bonding orbital and the d_{z^2} orbital of surface iridium atom. In addition, the first hydrogen atom abstraction of methane by the IrO_2(110) surface is a reaction with low barrier and high exothermic energy. The lower reaction barrier than the desorption energy indicates that the IrO_2(110) surface could provide not only high sticking coefficient but also high turnover frequency in methane dissociation reaction.

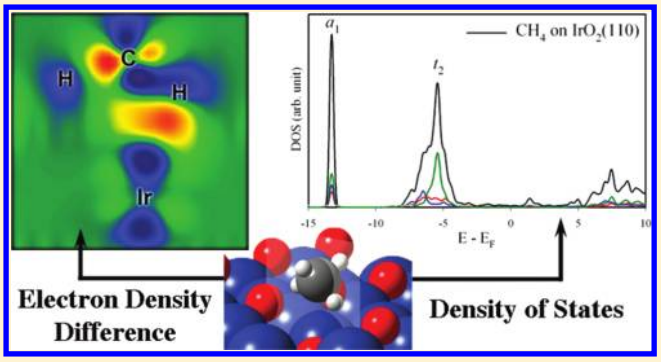

INTRODUCTION

Methane is the most abundant component of the natural gas; the high H/C ratio makes it containing highest energy per produced CO_2 equivalent. Methane is also a very important industrial raw material; it can be converted to higher hydrocarbons through the Fischer−Tropsch synthesis or used as starting material for the production of valuable petrochemical products.[1−3] Therefore, the methane dissociation or partial oxidation processes have led to a number of experimental[1−5] and theoretical[6−23] studies. However, the CH_4 molecule is geometrically high-symmetry and nonpolar, and it is neither electron donor nor acceptor; the special structural and electronic features of methane molecule make it weak interacted with catalytic surfaces. Recent DFT calculations also showed quite weak interactions (or no interaction) between methane and transition metal surfaces.[6,21] From a kinetic point of view, a higher adsorption energy of reactants leads to a higher turnover frequency in heterogeneous catalytic reactions. In our previous study, we calculated the adsorption of NH_x and N_2 on IrO_2(110) surfaces.[24] DFT calculated results showed that the inert N_2 molecule is strong bonded on the IrO_2(110) surface, and this result motivated us to check the interactions between the methane molecule and this surface.

Iridium dioxide, which crystallizes in the tetragonal rutile structure,[25] is a metal oxide that exhibits metallic conductivity at room temperature.[26] The stoichiometric IrO_2(110) surface [*s*-IrO_2(110)] presents exposed rows of 2-fold coordinated bridge oxygen atoms (O_{br}) and 5-fold coordinated Ir_{cus} atoms (cus = coordinatively unsaturated site) along the [001] direction. The (110)-oriented domain is one of the dominative surfaces of IrO_2;[27,28] this IrO_2(110) surface has been characterized in recent studies both experimentally and theoretically.[27,29] In this work, DFT was applied to calculate the adsorption of methane on the IrO_2(110) surfaces; the molecule−surface interactions were clearly characterized by analyses of density of states (DOS) and electron density difference. Moreover, the first hydrogen atom abstraction by the IrO_2(110) surface was calculated to predict the feasibility of further reactions of methane after the adsorption.

COMPUTATIONAL DETAILS

DFT calculations in this work were performed using the Vienna Ab-initio Simulation Package (VASP).[30−32] The generalized gradient approximation (GGA) was used with the functional described by Perdew and Wang[33] and a cutoff energy of 300 eV (1000 eV in DOS calculations). Spin-polarization calculations were performed for all of the structural optimizations; electron−ion interactions were investigated using the projector augmented wave method.[34] The IrO_2(110) surface was modeled as a two-dimensional slab in a 3D periodic cell. The slab was a 2 × 1 surface having the thickness of four O−Ir−O repeat units, equivalent to 12 atomic layers (Supporting Information). The upper seven atomic layers were relaxed in all structural optimizations. A 14 Å vacuum space was introduced to curtail interactions between the slabs. For this (2 × 1)-IrO_2(110) surface model, k-points of 3 × 3 × 1 were

Received: January 20, 2012
Revised: February 16, 2012
Published: February 23, 2012

   dx.doi.org/10.1021/jp300689j | *J. Phys. Chem. C* 2012, 116, 6367−6370

set by Monkhorst−Pack. The computational parameters and the surface model in this work have been recently applied to calculate the adsorptions and reactions on the $IrO_2(110)$ surfaces.[24,35] For transition state (TS) determination, the nudged elastic band (NEB) method, implemented in VASP, was applied. The validities of all the optimized structures and determined TSs were checked through normal-mode frequency analysis. To identify a real minimum on a potential energy surface, all frequencies had to be positive; a TS had to have one imaginary frequency corresponding to the reaction coordinate.

The estimated adsorption energy (E_{ads}) of the oxidation products was calculated using the formula

$$E_{ads} = E_{A/surf} - (E_{surf} + E_A)$$

where E_{surf} is the energy of the surface, E_A is the energy of the adsorbate, and $E_{A/surf}$ is the total energy of the adsorbate on the surface. A negative value of E_{ads} indicates an exothermic chemisorption process. The electron density difference (Q_{diff}) was calculated in a manner similar to the calculation of the binding energy:

$$Q_{diff} = Q_{A/surf} - (Q_{surf} + Q_A)$$

where Q_{diff} is the difference at each grid point in the total electron density matrix between that of the CH_4-bonded surface ($Q_{A/surf}$) and that of the sum of the surface (Q_{surf}) and the single CH_4 molecule (Q_A). According to this definition, positive and negative values of Q_{diff} correspond to increasing and decreasing electron densities, respectively.

RESULTS AND DISCUSSIONS

Figure 1 presents an atomic model of CH_4 adsorption on stoichiometric $IrO_2(110)$ surface. The CH_4 molecule attaches

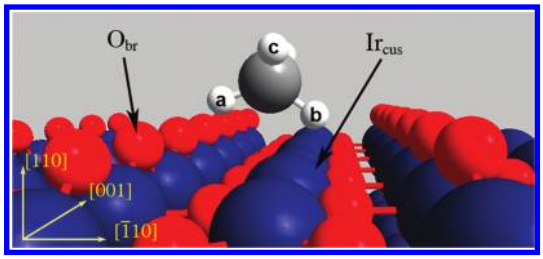

Figure 1. Ball-and-Stick model of the methane adsorption on the stoichiometric $IrO_2(110)$ surface.

to the surface via interacting with both O_{br} and Ir_{cus} atoms, and the adsorption energy (E_{ads}) is −0.41 eV. The strong interaction force between methane and the $IrO_2(110)$ surface results in a significantly longer $d(C-H_b)$, 1.16 Å, which is 0.06 Å longer than that of the free C−H bond. In addition, the $d(C-H_a)$ is also elongated by 0.02 Å. The adsorption energy and geometric parameters are summarized in Table 1. Because of the geometrically high symmetry of the CH_4 molecule, it is difficult for methane to interact with most of catalytic materials. On the *s*-$IrO_2(110)$ surface, however, the adsorption energy of methane is surprisingly high and much higher than those on transition metal surfaces,[6,8,20−23,36] oxygen precovered metals,[21] and other different type of catalysts.[10,16] In this work, we also calculated the adsorption of methane on the stoichiometric $RuO_2(110)$ and $TiO_2(110)$ surfaces for comparison,[37] and Table 1 lists the adsorption energies and selected geometric parameters of methane adsorptions.

Table 1. Adsorption Energy (eV) and Selected Geometric Parameters (Å) of CH_4 Adsorption on Stoichiometric $IrO_2(110)$, $RuO_2(110)$, and $TiO_2(110)$ Surfaces

	s-$IrO_2(110)$	*o*-$IrO_2(110)$	*s*-$RuO_2(110)$	*s*-$TiO_2(110)$
E_{ads}	−0.41	−0.63	−0.18	−0.06
$d(C-H_a)$	1.12	1.10	1.10	1.10
$d(C-H_b)$	1.16	1.17	1.12	1.10
$d(C-H_c)$	1.10	1.10	1.10	1.10
$d(O_{br}...H_a)$	2.11	2.14	2.20	2.71
$d(O_{cus}...H_c)$		2.52		
$d(M_{cus}...H_b)^a$	1.88	1.87	2.34	3.15

[a] *M* = Ir, Ru, or Ti.

For the methane adsorption on stoichiometric $RuO_2(110)$ and $TiO_2(110)$ surfaces, the adsorption energy are −0.18 and −0.06 eV, respectively. The CH_4 molecule on the $RuO_2(110)$ surface still has a weak adsorption energy, and there is almost no interaction when it adsorbs on the $TiO_2(110)$ surface. This energetic trend of adsorption energies is the same as previous study in N_2 adsorption;[24] we believe that the high activity of the $IrO_2(110)$ surface in methane adsorption, again, comes from the special electronic structure of Ir_{cus} atoms. In our previous study about the N_2 adsorption on rutile crystallized metal oxide surfaces,[24] we found that the continuous d_z^2 band that across the Fermi energy induces a high reactivity of the Ir_{cus} atom with the lone pair of the N_2 molecule on the $IrO_2(110)$ surface; for $RuO_2(110)$ and $TiO_2(110)$ surfaces, the d_z^2 bands farther away from the Fermi level results in lower N_2 adsorption energies.[24] In this study, however, the Ir_{cus} atom interacts with the C−H bonding orbital without lone pair and still demonstrates a high activity in bond formation. Figure 2 shows the electron density

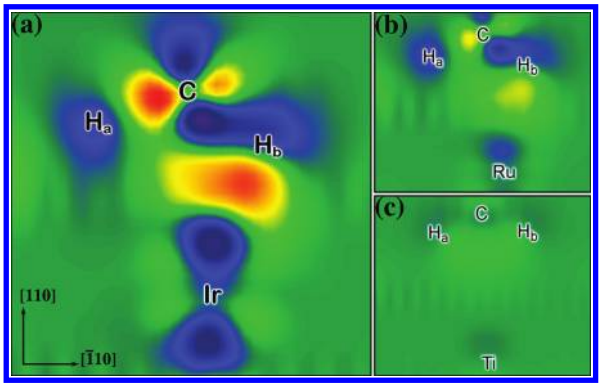

Figure 2. Electron density difference contour plot of CH_4 adsorptions on: (a) $IrO_2(110)$, (b)$RuO_2(110)$, and (c) $TiO_2(110)$ surfaces. The red and blue colors represent the increasing and decreasing electron densities, respectively.

difference contour map of CH_4 adsorption on the three rutile crystallized surface. The contour surfaces are aligned normal to the [001] direction and cut through the CH_4 bonded M_{cus} (M = Ir, Ru, or Ti) atom. In part a of Figure 2, the contour plot of the adsorption on the *s*-$IrO_2(110)$ surface, a wide electron density increasing region (red color) between the molecule and the surface clearly demonstrates the interaction among the σ bond of $C-H_b$ and the Ir_{cus} atom. Furthermore, this interaction simultaneously induces a weakening of $C-H_b$ bond and the electron density loss from the d_z^2 orbital of Ir_{cus} atom. In parts b and c of Figure 2, the contour plots of methane adsorption on the $RuO_2(110)$ and $TiO_2(110)$ surface consists with the

dx.doi.org/10.1021/jp300689j | J. Phys. Chem. C 2012, 116, 6367−6370

corresponding adsorption energies, that is lower interaction energy with fewer electron density difference induced.

In addition, we calculated the DOS of the methane adsorption on the stoichiometric $IrO_2(110)$ surface to characterize the interactions. Part a of Figure 3 shows the DOS of CH_4 molecule adsorbed on the *s*-$IrO_2(110)$ surface. Here, we used four hydrogen s orbitals to represent the hybridized CH_4 molecular orbitals. The triplet t_2 state of methane is split into three isolated states after the interaction. The four degenerate C−H bonding orbitals are clearly separated into three groups: O_{br} bonded H_a, Ir_{cus} bonded H_b, and two noninteracted free H atoms. For the strong interacted C−H_b bond, a high magnitude of delocalization can be found on the H_b atom (blue line) in part a of Figure 3. In addition, part b of Figure 3 shows the DOS difference of d_z^2 orbital of the Ir_{cus} atom before and after the adsorption of methane; this DOS difference plot clearly demonstrates that the d_z^2 state of Ir_{cus} atom participates in the bond formation with the CH_4 molecule. In part b of Figure 3, the d_z^2 states near Fermi energy are delocalized (blue filled area) and shifted to higher energy level (yellow filled area), and part of them are shifted to ca. −6 and −13 eV. The new generated d_z^2 states are clearly overlapped with the CH_4 molecular states in part a of Figure 3; although the degree of overlapping is not high (due to the weak σ−d interaction), it reveals the existence of the interaction between the Ir_{cus} atom and methane, and is consistent with the results from electron density difference contour plot in part a of Figure 2.

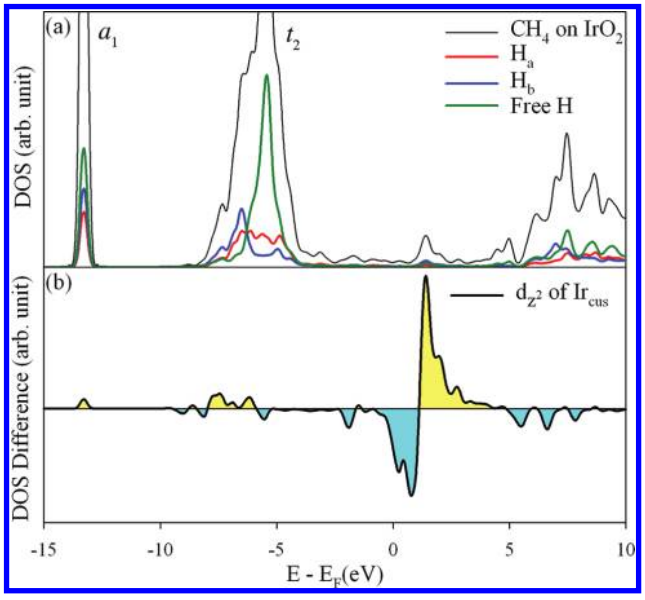

Figure 3. (a) DOS of the CH_4 molecule adsorbed on $IrO_2(110)$ surface, and projected DOS of four hydrogen atoms. (b) DOS difference in d_z^2 state of Ir_{cus} atom before and after the CH_4 adsorption.

From the DOS plot in part a of Figure 3, we can see that the magnitude of delocalization of the H_a atom (red line) is similar to H_b atom (blue line), which implies the hydrogen bonding force between the CH_4 molecule and the O_{br} atom is also an important factor that leading to a high adsorption energy. Here, we calculated the methane adsorption on the oxygen-rich $IrO_2(110)$ surface [*o*-$IrO_2(110)$] to verify the effect of lateral interactions; the oxygen-rich surface denotes to additional oxygen atoms, O_{cus}, adsorb on the Ir_{cus} sites. In our previous investigation of the NH_x adsorption on the $IrO_2(110)$ surfaces,[24] the existence of O_{cus} atoms is a significant factor that increases adsorption energies of adsorbates. Moreover, the core-level spectroscopy study by Chung et al.[29] showed that the O_{cus} atom is an active and long-lived species on the $IrO_2(110)$ surface. For the methane adsorption on the *o*-$IrO_2(110)$ surface, two lateral interactions with O_{cus} atoms[38] stabilized the CH_4 molecule with a adsorption energy of −0.63 eV (geometrical parameters are listed in Table1). To the best of our knowledge, this is the highest adsorption energy of methane in heterogeneous catalytic system that had been investigated. The high adsorption energy also indicates that the sticking coefficient of methane on the $IrO_2(110)$ surface could be higher than other catalytic surfaces.

Besides the DOS and electron density difference analyses of the adsorption, we also calculated the hydrogen atom abstraction of methane by the stoichiometric $IrO_2(110)$ surface. Figure 4 presents structures of the transition state and the final state of this hydrogen atom abstraction, and the corresponding geometric parameters are listed in the Supporting Information. In the hydrogen abstraction process, H_b atom of methane migrates to the neighbor O_{br} atom and the methyl group binds to the Ir_{cus} atom. The corresponding energy barrier ($E^{\ddagger}$) is 0.30 eV, and the reaction energy (ΔE) is −1.09 eV before the zero-point energy (ZPE) correction.[39] The reaction coordinate of this C−H dissociation is directly coupled to the C−H stretching mode in this methane dehydrogenation and leads to a high imaginary frequency (1246 cm^{-1}) at the transition state and large ZPE correction to reaction barrier. After the ZPE correction, the barrier $E^{\ddagger}_{ZPE}$ is lowered to 0.18 eV, and the corrected reaction energy ΔE_{ZPE} is −1.06 eV. According to our

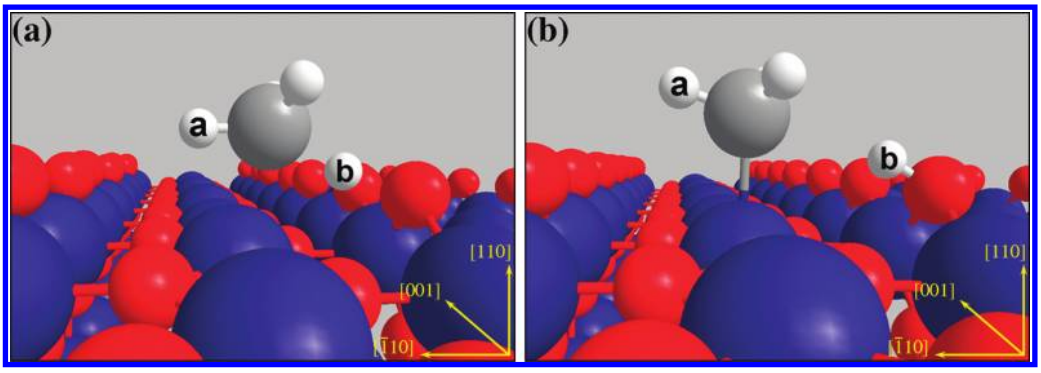

Figure 4. Ball-and-Stick model of (a) transition state, and (b) final state of the hydrogen atom abstraction by the stoichiometric $IrO_2(110)$ surface.

dx.doi.org/10.1021/jp300689j | *J. Phys. Chem. C* 2012, 116, 6367−6370

calculation, the barrier of hydrogen abstraction by the *s*-$IrO_2(110)$ surface is significantly lower than the desorption energy of methane; in other words, the adsorbed methane molecules prefer C−H dissociation rather than desorption on the *s*-$IrO_2(110)$ surface. Moreover, the high exothermic energy of the hydrogen atom abstraction reaction indicates that the reverse reaction is relatively unfavorable. For the abstraction by the *o*-$IrO_2(110)$ surface, the hydrogen abstraction by the O_{cus} atom is not favorable because the final state of this reaction is not stable. Therefore, the hydrogen atom abstraction reaction on the oxygen-rich surface is similar to the that on the stoichiometric surface−dehydrogenation to the O_{br} atom. The reaction barrier of the hydrogen atom abstraction by the *o*-$IrO_2(110)$ surface is 0.33 eV, and the reaction energy is −0.83 eV. This barrier is very close to that by the stoichiometric surface, but a stronger binding energy of methane on the oxygen-rich surface makes the forward dissociation a more preferred reaction. Comparing with recent DFT studies about methane dissociation,[11,19] a reaction barrier of 0.30 eV is not the lowest one, but a higher methane−surface desorption energy than the dissociation barrier has never been found; that is, a high turnover frequency from CH_4 to CH_3 could be reached on the $IrO_2(110)$ surface.

CONCLUSIONS

In summary, we found a special interaction in the adsorption of methane on the $IrO_2(110)$ surfaces. Both analyses of electron density difference and DOS show a significant interaction between the C−H bonding orbital and the d_z^2 state of the Ir_{cus} atom. This σ−d interaction combined with hydrogen bonding forces with surface oxygen species, O_{br} and O_{cus}, results in a high adsorption energy of methane on the $IrO_2(110)$ surfaces. In addition, it shows a low reaction barrier and high exothermic energy for the hydrogen atom abstraction by $IrO_2(110)$ surfaces. Our calculations demonstrate that the $IrO_2(110)$ surface could be a potential catalyst for methane dissociation reactions due to the high sticking coefficient and high turnover frequency of methane on the $IrO_2(110)$ surface.

ASSOCIATED CONTENT

Supporting Information

Layer definition of the supercells in this work, top view of methane adsorption on the oxygen-rich $IrO_2(110)$ surface, selected geometric parameters of transition state, and final state of the hydrogen atom abstraction reaction, and the potential energy surface of the adsorption and reaction in this work. This material is available free of charge via the Internet at http://pubs.acs.org.

AUTHOR INFORMATION

Corresponding Author

*E-mail: jcjiang@mail.ntust.edu.tw, Tel: +886-2-27376653, Fax: +886-2-27376644.

Notes

The authors declare no competing financial interest.

ACKNOWLEDGMENTS

We thank the National Science Council of Taiwan (NSC 98-2113-M-011-001-MY3) for supporting this research financially and the National Center of High-Performance Computing for computer time and facilities.

REFERENCES

(1) Dave, N.; Foulds, G. A. *Ind. Eng. Chem. Res.* **1995**, *34*, 1037.
(2) Pitchai, R.; Klier, K. *Catal. Rev.* **1986**, *28*, 13.
(3) Amenomiya, Y.; Birss, V. I.; Goledzinowski, M.; Galuszka, J.; Sanger, A. R. *Catal. Rev. − Sci. Eng.* **1990**, *32*, 163.
(4) Juurlink, L. B. F.; McCabe, P. R.; Smith, R. R.; DiCologero, C. L.; Utz, A. L. *Phys. Rev. Lett.* **1999**, *83*, 868.
(5) Gee, A. T.; Hayden, B. E.; Mormiche, C.; Kleyn, A. W.; Riedmüller, B. *J. Chem. Phys.* **2003**, *118*, 3334.
(6) Au, C. T.; Ng, C. F.; Liao, M. S. *J. Catal.* **1999**, *185*, 12.
(7) Ciobica, I. M.; Frechard, F.; van Santen, R. A.; Kleyn, A. W.; Hafner, J. *J. Phys. Chem. B* **2000**, *104*, 3364.
(8) Ciobica, I. M.; van Santen, R. A. *J. Phys. Chem. B* **2002**, *106*, 6200.
(9) Zhang, C. J.; Hu, P. *J. Chem. Phys.* **2002**, *116*, 322.
(10) Zhang, C. J.; Hu, P. *J. Chem. Phys.* **2002**, *116*, 4281.
(11) Liu, Z. P.; Hu, P. *J. Am. Chem. Soc.* **2003**, *125*, 1958.
(12) Anghel, A. T.; Wales, D. J.; Jenkins, S. J.; King, D. A. *Phys. Rev. B* **2005**, *71*, 113410.
(13) Bunnik, B. S.; Kramer, G. J. *J. Catal.* **2006**, *242*, 309.
(14) Knapp, D.; Ziegler, T. *J. Phys. Chem. C* **2008**, *112*, 17311.
(15) Nave, S.; Tiwari, A. K.; Jackson, B. *J. Chem. Phys.* **2010**, *132*, 054705.
(16) Blanco-Rey, M.; Jenkins, S. *J. Chem. Phys.* **2009**, *130*, 014705.
(17) van Grootel, P. W.; van Santen, R. A.; Hensen, E. J. M. *J. Phys. Chem. C* **2011**, *115*, 13027.
(18) Chin, Y. H.; Buda, C.; Neurock, M.; Iglesia, E. *J. Catal.* **2011**, *283*, 10.
(19) Mayernick, A. D.; Janik, M. J. *J. Catal.* **2011**, *278*, 16.
(20) Kokalj, A.; Bonini, N.; Sbraccia, C.; de Gironcoli, S.; Baroni, S. *J. Am. Chem. Soc.* **2004**, *126*, 16732.
(21) Xing, B.; Pang, X. Y.; Wang, G. C. *J. Catal.* **2011**, *282*, 74.
(22) Gajewski, G.; Pao, C. W. *J. Chem. Phys.* **2011**, *135*, 064707.
(23) Kinnunen, N. M.; Hirvi, J. T.; Suvanto, M.; Pakkanen, T. A. *J. Phys. Chem. C* **2011**, *115*, 19197.
(24) Wang, C.-C.; Siao, S. S.; Jiang, J. C. *J. Phys. Chem. C* **2010**, *114*, 18588.
(25) Mattheiss, L. F. *Phys. Rev. B* **1976**, *13*, 2433.
(26) Ryden, W. D.; Lawson, A. W. *Phys. Rev. B* **1970**, *1*, 1494.
(27) He, Y. B.; Stierle, A.; Li, W. X.; Farkas, A.; Kasper, N.; Over, H. *J. Phys. Chem. C* **2008**, *112*, 11946.
(28) Chen, R. S.; Chang, H. M.; Huang, Y. S.; Tsai, D. S.; Chattopadhyay, S.; Chen, K. H. *J. Cryst. Growth* **2004**, *271*, 105.
(29) Chung, W. H.; Wang, C. C.; Tsai, D. S.; Jiang, J. C.; Cheng, Y. C.; Fan, L. J.; Yang, Y. W.; Huang, Y. S. *Surf. Sci.* **2010**, *604*, 118.
(30) Kresse, G.; Hafner, J. *Phys. Rev. B* **1993**, *48*, 13115.
(31) Kresse, G.; Furthmuller, J. *Phys. Rev. B* **1996**, *54*, 11169.
(32) Kresse, G.; Furthmuller, J. *Comput. Mater. Sci.* **1996**, *6*, 15.
(33) Perdew, J. P. In *Electronic Structure of Solids '91*; Ziesche, P., Eschrig, H., Eds.; Akademie Verlag: Berlin, 1991; p 11.
(34) Kresse, G.; Joubert, D. *Phys. Rev. B* **1999**, *59*, 1758.
(35) Wang, C.-C.; Siao, S. S.; Jiang, J. C. *Langmuir* **2011**, *27*, 14253.
(36) Xing, B.; Pang, X. Y.; Wang, G. C.; Shang, Z. F. *J. Mol. Catal. A: Chem.* **2010**, *315*, 187.
(37) The computational parameters and the surface model in *J. Phys. Chem. C* 2009, *113*, 2816 was adopted for calculations on the $RuO_2(110)$ surface. For the calculations on $TiO_2(110)$ surface, the surface model was also a 2 × 1 slab model with the same layer thickness and vacuum space in this work; it was calculated using the same computational settings described herein.
(38) Since the surface model applied in this work is a 2 × 1 slab, both neighbored Ir_{cus} site will be occupied by the O_{cus} atom in the calculation of CH_4 adsorption on the *o*-$IrO_2(110)$ surface. The top view of the methane adsorption on the *o*-$IrO_2(110)$ surface are shown in Figure S2 of the Supporting Information.
(39) The values of the barrier and reaction energy are relative to the adsorption state of methane. The potential energy surface of the methane adsorption and the hydrogen atom abstraction is shown in Figure S3 of the Supporting Information.